POLITECNICO DI TORINO
Repository ISTITUZIONALE

Single Scans of Ti-6Al-4V by Directed Energy Deposition: A Cost and Time Effective Methodology to Assess the Proper Process Window

Original
Single Scans of Ti-6Al-4V by Directed Energy Deposition: A Cost and Time Effective Methodology to Assess the Proper Process Window / Carrozza, Alessandro; Mazzucato, Federico; Aversa, Alberta; Lombardi, Mariangela; Bondioli, Federica; Biamino, Sara; Valente, Anna; Fino, Paolo. - In: METALS AND MATERIALS INTERNATIONAL. - ISSN 1598-9623. - ELETTRONICO. - (2021). [10.1007/s12540-020-00930-3]

Availability:
This version is available at: 11583/2866792 since: 2021-03-11T12:40:28Z

Publisher:
Springer

Published
DOI:10.1007/s12540-020-00930-3

Terms of use:

This article is made available under terms and conditions as specified in the corresponding bibliographic description in the repository

Publisher copyright

(Article begins on next page)

12 October 2024

Metals and Materials International
https://doi.org/10.1007/s12540-020-00930-3

Single Scans of Ti-6Al-4V by Directed Energy Deposition: A Cost and Time Effective Methodology to Assess the Proper Process Window

Alessandro Carrozza[1] · Federico Mazzucato[2] · Alberta Aversa[1] · Mariangela Lombardi[1] · Federica Bondioli[1] · Sara Biamino[1] · Anna Valente[2] · Paolo Fino[1]

Received: 26 September 2020 / Accepted: 16 November 2020
© The Author(s) 2021

Abstract
Directed energy deposition is an additive manufacturing technology which usually relies on prototype machines or hybrid systems, assembled with parts from different producers. Because of this lack of standardization, the optimization of the process parameters is often a mandatory step in order to develop an efficient building process. Although, this preliminary phase is usually expensive both in terms of time and cost. The single scan approach allows to drastically reduce deposition time and material usage, as in fact only a stripe per parameters combination is deposited. These specimens can then be investigated, for example in terms of geometrical features (e.g. growth, width) and microstructure to assess the most suitable process window. In this work, Ti-6Al-4V single scans, produced by means of directed energy deposition, corresponding to a total of 50 different parameters combinations, were analyzed, focusing on several geometrical features and relative parameters correlations. Moreover, considering the susceptibility of the material to oxygen pick-up, the necessity of an additional shielding gas system was also evaluated, by comparing the specimens obtained with and without using a supplementary argon flow. A process window, which varies according to the user needs, was found together with a relationship between microstructure and process parameters, in both shielding scenarios.

Keywords Additive manufacturing · Directed energy deposition · Titanium alloys · Ti-6Al-4V

✉ Alessandro Carrozza
alessandro.carrozza@polito.it

Federico Mazzucato
federico.mazzucato@supsi.ch

Alberta Aversa
alberta.aversa@polito.it

Mariangela Lombardi
mariangela.lombardi@polito.it

Federica Bondioli
federica.bondioli@polito.it

Sara Biamino
sara.biamino@polito.it

Anna Valente
anna.valente@supsi.ch

Paolo Fino
paolo.fino@polito.it

[1] Department of Applied Science and Technology, Politecnico di Torino, C.so Duca degli Abruzzi 24, 10129 Turin, Italy

[2] SUPSI, Institute of Systems and Technologies for Sustainable Production, Galleria 2, 6928 Manno, Switzerland

1 Introduction

Directed Energy Deposition (DED) is a laser-based Additive manufacturing (AM) technology which allows the production of metallic components from a feedstock material, usually in the form of prealloyed powder [1]. DED techniques differ from Powder Bed Fusion (PBF) systems mainly due to the material disposition method: while the former implies the delivery of the powder through carrier gas from nozzles directly on the building platform, in the latter, a layer of powder completely covers the whole platform each time a new layer is added [2]. PBF technologies, such as Laser Powder Bed Fusion (LPBF), grant the possibility to build more complex components, characterized by a lower surface roughness, when compared to DED [3]. Nonetheless, DED allows building rates more than 10 times greater, in addition to the ability to manufacture bigger components [4]. DED is also well-suited for some specific applications, such as remanufacturing/repairing of pre-existing pieces and graded-materials production [3].

Published online: 25 January 2021

To achieve a wide-spread diffusion of this technology, the optimization of the process parameters is a mandatory step in order to guarantee the desired component's properties, for example in terms of shape stability and mechanical properties. This operation is in general a critical aspect of AM technologies, in particular for DED, which usually relies on prototypes, custom-made machines or systems assembled with different commercially available parts [5–7]. Even if fundamental, process optimization is a time-consuming procedure, that usually involves the production of a large number of samples to be characterized. Although, the process parameters determination is far from being a standardized procedure, as confirmed by a relevant number of works available in literature on this field, in which different determining parameters were used to conduct the optimization [8–10]. For example, Kobryn et al. [8] evaluated the effect of variations in laser power and traverse speed on Ti-6Al-4V samples, in terms of porosity, microstructure and sample's height. Instead, Mahamood et al. [10] focused of the effect of these process parameters on hardness, chosen as the determining property in order to select the most suitable parameters combination. Most of the articles in literature share the use of 3D samples, which production results expensive both economically and in terms of time.

A more cost-effective approach consists in studying single scans (or single beads), drastically reducing the amount of feedstock material required and the overall job time. Of course, the effect of process parameters related to multiple meltpool interactions, such as hatching distance and layer height, cannot be evaluated this way. Although this method results very useful to assess the influence of laser power, scanning speed and environmental factors (e.g. shielding flow). The single scan approach for DED was already successfully used in several works using disparate materials. For example, Peng et al. [11] optimized the deposition of a nickel alloy produced by means of DED, using single scans to better investigate meltpools. Different geometrical features, such as the height and width, were evaluated in this work. Although the authors obtained cracked specimens in all the conditions considered for this experiment, probably due to the high levels of oxygen/residual stress in the samples. Therefore, the authors determined the most appropriate processing condition by building larger samples (single layer and 3D) and taking into considerations other criteria, such as the stability of the height value of the whole specimen. A similar evaluation was conducted by Mazzucato et al. [12] in a work aimed at determining the influence of different scanning strategies on the quality of AISI 316L samples. In this study, the most suitable process parameters were successfully determined by performing a stability investigation. To do so, the on-top views of several single scans were analyzed and categorized according to their morphology. Then, the most promising process parameters were determined by analyzing the cross-sections and selecting the samples characterized by a low porosity and proper substrate remelting. Aversa et al.[13] used a similar approach for AlSi10Mg single scans. In this work, the authors were able to correlate the stability and geometrical features of the scans to the process parameters used. The most proper process window was also determined, suggesting the single scan approach as a useful tool in order to investigate new powder compositions in the future.

Concerning Ti-6Al-4V DED single scans, only a few works are available in literature. Gockel et al. [14] investigated single lines deposition in order to evaluate the effect of a change in process parameters on microstructure and meltpool size, although only through simulations. Instead, Katinas et al. [15] investigated Ti-6Al-4V single scans, but the aim of the study was to evaluate laser capture efficiency only, without focusing on the properties of the part built.

Titanium alloys, particularly Ti-6Al-4V, are optimal materials to be produced by means of DED, mainly due to the high costs associated to process these alloys using conventional technologies and to their use in some specific industrial sectors, in which small production volumes and high-quality components are required, such as the aerospace fields [4, 16–19]. Arcella et al. [20] assessed the most critical properties for titanium alloys commonly used in the aerospace industries. As regards in particular DED-produced samples, these properties resulted similar, if not superior, to the conventionally manufactured counterparts, in addition showing a projection of cost savings of 15%–30%. Therefore, DED appears an effective technology both in terms of mechanical properties achieved and cost effectiveness for this material.

Titanium alloys are also very susceptible to oxygen pick-up and oxidation, which results in several difficulties during processing [17, 21]. Conducting the deposition in a sealed and controlled environment (glovebox-like) ensures a more cautious process. Although this strongly limits the maximum component size reachable, which is one of the most promising features of the DED technology, not being the machines limited to the size of the process chamber, such as in LPBF [22]. Works conducted both is a sealed [23] and open environment [24] are available in literature. In the second scenario, a complementary shielding system is usually adopted in order to prevent excessive oxygen enrichment in the alloy. The shielding gas mass flow is then another important parameter to be optimized: it must be kept as low as possible, due to the high cost of the inert gas, usually argon, [25] but high enough to prevent the embrittlement of the component [26].

In this work, the single scan approach, through geometrical features and related parameters evaluation, was adopted in order to find the most suitable process window (laser power, scanning speed) to process the Ti-6Al-4V alloy by means of

DED. The fabrication process was not conducted in a sealed environment, instead an additional shielding gas system was used. Therefore, the effect of the shielding gas stream was also assessed by evaluating the influence of the argon flow variations on the quality of the samples, in terms of both geometry and microstructure. This last investigation is fundamental in order to assess the applicability of an open environment, a promising feature for big components production, to titanium alloys, notoriously susceptible to oxygen/nitrogen pick-up. Furthermore, powder efficiency was also used as a criterion in order to further discern the optimized process parameters. In the end, the influence of the process on the microstructure was also studied and incorporated in the process map.

2 Materials and Methods

In this work, a Ti-6Al-4V ELI gas atomized powder (LPW Technology Ltd.) was used in order to build several 20 mm long single scans on a Ti-6Al-4V substrate. Further information on the powder can be found elsewhere [21]. The samples were produced in SUPSI (University of Applied Sciences and Arts of Southern Switzerland) laboratory (ARM lab – DTI), using a Laserdyne®430 system, characterized by a maximum laser power (P) of 1000 W, wavelength (λ) of 1070 nm and laser spot (D) of 1 mm. A multi-nozzle deposition head, provided by Optomec, was employed. Further details on the system are available in the authors previous work [12]. In order to increase theprotectionof the deposition area from oxidation, the deposition head was equipped with an external circular device capable of providing a homogeneous supply of extra inert gas surrounding the melt pool for a total area of 89 mm in diameter. Argon (purity 4.6) was used as a carrier and shielding gas, using a flow of 4 l/min and 15 l/min, respectively.

Five different values of laser power (P) and ten of scanning speed (v) were investigated, as illustrated in Table 1, for a total of 50 total combinations. All the specimens were built using a constant powder feed rate (F) of 0.017 g/s.

Moreover, in order to analyze the effect of the shielding gas, all the specimens were built in two different environmental conditions: without the additional shielding gas system (**ArS0**) and using an additional flow of 15 l/min (**ArS15**).

On-top imaging was performed using a Leica EZ4W stereomicroscope, in order to study the morphology of the single tracks. The specimens were then cut perpendicularly to the scan direction at half length, in order to analyze a section where the steady state is reached. Then mounted, polished and etched employing a Kroll solution (93% H_2O, 5% HNO_3, 2% HF). The cross-sections were investigated employing a Leica DMI 5000 M optical microscope. The geometrical features were evaluated using an image analysis program. In order to quantify the microstructures, the same program was used to evaluate α' spacing (σ_t), using the methodology described by *Vander Voort* [27] for evaluating the interlamellar spacing of paerlite in steels. Based on this method, for each sample, 15 different micrographs were studied by superimposing a circular grid, which diameter value was known (d_c), and counting the number of times the edge of an α' needle intersected the circle (n). The use of a circular grid allows to obtain more accurate results, with respect of a straight line, when evaluating features oriented in multiple directions.

The average spacing is then evaluated as:

$$\sigma_t = \frac{1}{2N_L} = \frac{\pi d_c}{2n} \tag{1}$$

where N_L is the number of intersections per unit length of test line.

This methodology was already applied to titanium alloys by Galarraga et al. [28], who used it in order to evaluate α-lath thickness (σ_t) in Ti-6Al-4V samples produced by means of electron beam melting. In this work, this procedure was used to determine the average spacing between α' needles, instead of α laths. This is a good indicator as a lower spacing corresponds to a higher martensitic density, hence a finer microstructure.

3 Results and Discussion

The on-top and cross-section analysis of the single scans built using different process parameters combinations allowed to determine the most critical samples: whilst most specimens were characterized by homogeneous track, suggesting a stable deposition phase, the ones built using a laser power of 100 W resulted highly irregular, as illustrated in Fig. 1. This is mostly due to incomplete melting of the feedstock powder and the baseplate. In fact, the unmelted particles resulted clearly visible on the baseplate (e.g. v = 300 mm/min, ArS15 in Fig. 1). Moreover, for higher scanning speed values, melting resulted so inefficient that the resulting sample merely comprised feedstock material, in the form of sparse particle attached to the baseplate (e.g. v = 1200 mm/min, ArS15 in Fig. 1). Even if the 100 W scans built using the lowest scanning speed are considered, a poor adhesion between the track itself and the baseplate is clear from the cross-section view. Moreover, interfacial delamination is noted (e.g. v = 150 mm/min, ArS15 in Fig. 1).

Table 1 Discrete process parameters values used to obtain all the analysed combinations

P (W)	v (mm/min)
100, 300, 500, 700, 900	150, 300, 450, 600, 750, 900, 1050, 1200, 1350, 1500

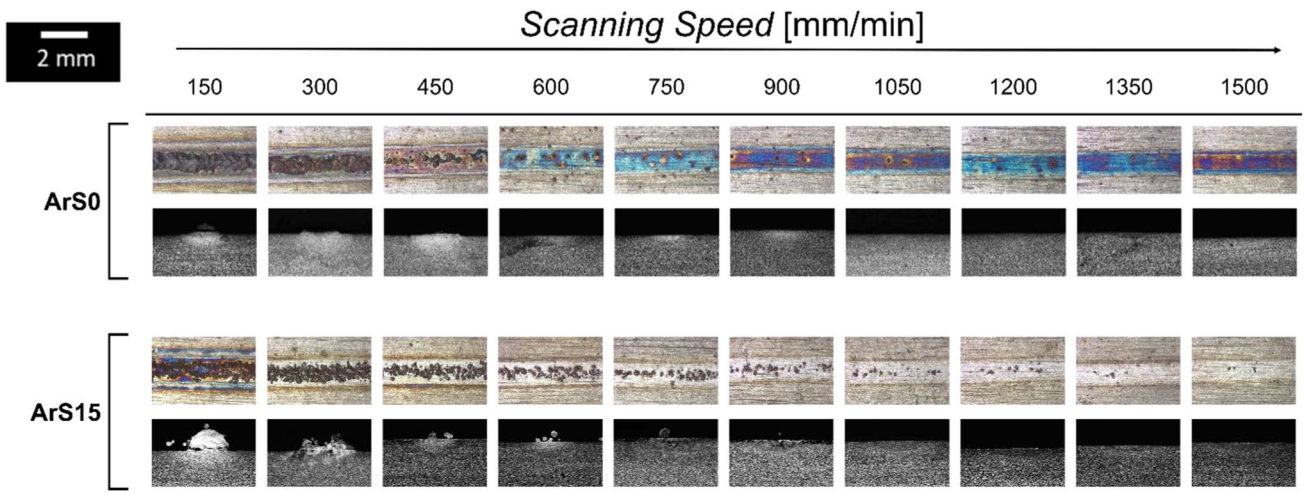

Fig. 1 On-top and cross-section view of the irregular scans built using P = 100 W, both with and without additional shielding. The scalebar is provided in the upper-left part of the image

As a consequence of the low deposition rate and the highly defective scan-platform interface, the specimens built using a laser power of 100 W were not considered for further analysis, as the related set of parameters would certainly lead to low quality 3D samples.

From the on top analyses of the samples produced with higher power, surface oxidation visibly varied between the samples as a result of different process parameters being applied (laser power, scanning speed and shielding gas flow), as illustrated in Fig. 2.

The ArS0 samples were characterized by a colorful external surface for either high and low values of P and v, as visible in Fig. 2a. This property is often correlated with oxidation. In particular, different previous works available in literature [29, 30] correlate α + β titanium alloys surface color to the temperature at which the oxidation occurred. Surfaces ranging from golden to blue-purple, as in Fig. 2a, are obtainable as result of heating up the sample at 500–650 °C. These kinds of oxides are usually the result of the presence of a mixture of different phases, such as TiO, TiO_2 and Ti_2O_3. Surfaces of these types are considered unacceptable for welding applications, due to the excessive oxygen pick-up [30, 31]. Even if the visual inspection of the color of the sample is a qualitative analysis, the American Welding Society provided two specifications for fusion welding in the aerospace industry, in which this methodology is suggested in order to assess the excessive oxidation of titanium welds [32]. Instead, the ArS15 samples built deploying the same set of building parameters, showed a much greater regularity in surface color, as visible in Fig. 2b. These specimens provided more reflective surfaces, suggesting a less severe oxidation. Moreover, the oxidation can be clearly detected also by investigating the samples of the P = 100 W series (Fig. 1), characterized by poor melting of the feedstock powder. When the additional argon flow is lacking, the substrate itself became colorful as a result of the effect of the laser, whilst this phenomenon did not happen significantly in presence of additional shielding (Fig. 1). Therefore, the additional inert gas flow is beneficial in terms of protection from oxidation, granting the possibility to build scans characterized by a limited amount of critical oxide layers.

The single scans cross-sections images were furtherly analyzed, as schematized in Fig. 3, by evaluating different geometrical features, such as its width (W), growth (G) and depth (D).

To further understand the influence that process parameters had on these geometrical features, W, G and D were plotted as a function of the linear energy density (LED), which can be used a single parameter to evaluate at the same time the influence of laser power (P) and scanning speed (v). In fact, it was calculated as:

$$LED = \frac{P}{v} \tag{2}$$

The outcomes of the geometrical feature analysis are provided in Fig. 4.

W variations were positive as LED increased in both shielding conditions. In particular, when comparing samples built using the same laser power, larger scans were associated to higher LED values. For low to intermediate LED values (LED < 200 J/mm), the curves relative to the samples built using a P of 700 W and 900 W were overlapped, suggesting a power threshold value over which width cannot significantly increase by just changing P. The beneficial effect of an increase in LED on W might be caused by the improved effectiveness of the system to melt the feedstock powder, when a higher energy density is used. This

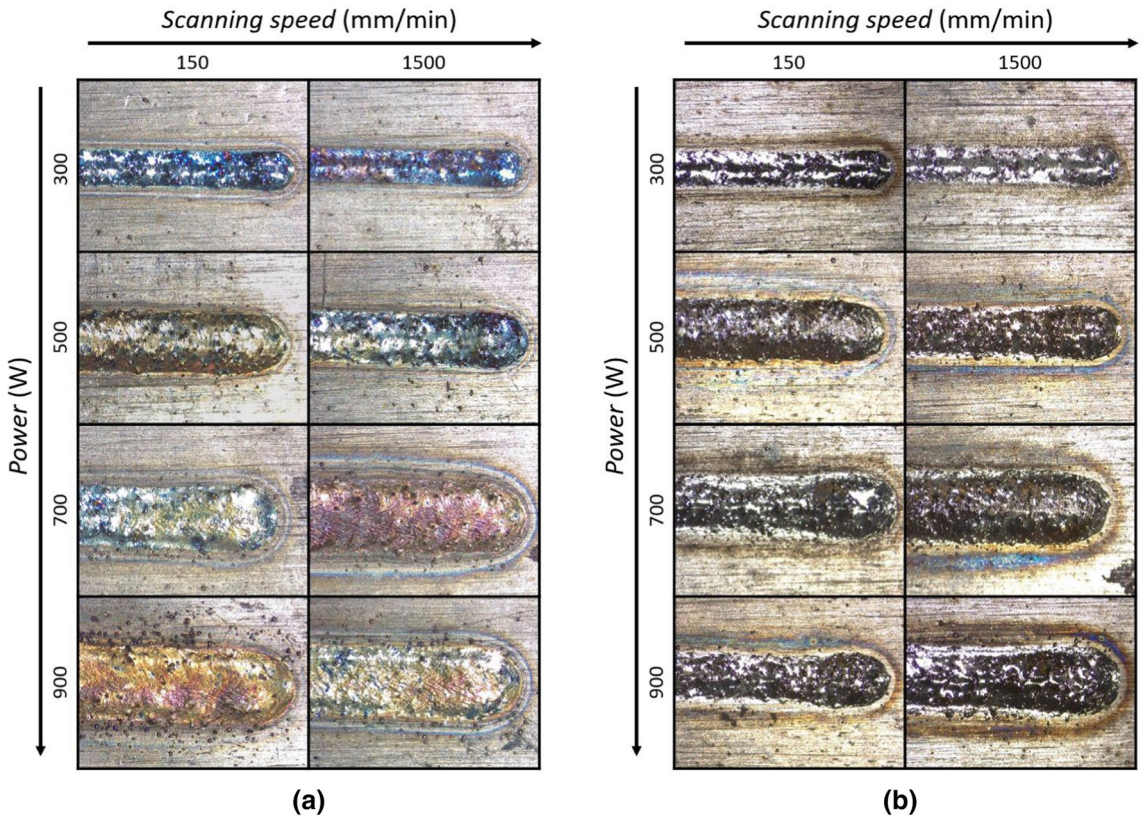

Fig. 2 On-top view of ArS0 **a** and ArS15 **b** single scans built using different process parameters

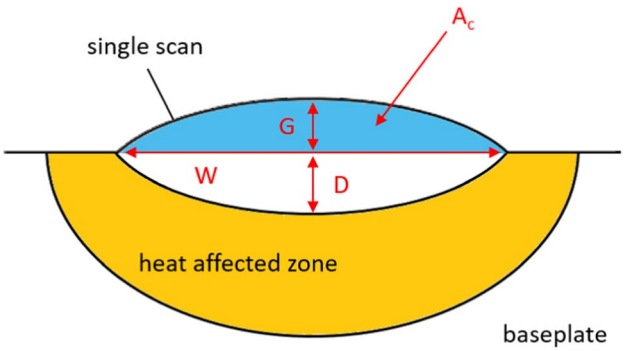

Fig. 3 Schematic representation of the geometrical features evaluated on a single scan cross-section

suggests that more material is effectively melted, granting larger scans.

G showed a different behavior, with respect to W. In fact, the relative trends were steeper when corresponding to lower laser power values. However, higher P values allowed to reach higher LEDs, which provided more consistent growths, similarly to the previous case.

D, instead, showed a variation similar to W, although a threshold power value was not detected, and the slope decreased significantly at high LED values. Moreover, for low P values (300, 500 W) the ArS15 samples showed higher depths, whilst this difference became negligible for higher P values (700, 900 W).

When comparing the results of these geometrical features in terms of the effect of the additional shielding gas, negligible variations of W (< 10%) were detected. Instead, G and D showed an increase in ArS15 samples, particularly at higher LED values, meaning that the lack of additional shielding gas impacts more on the samples built using high power and low scanning speed.

The majority of the samples provided very negligible porosities, which is the reason why porosity minimization was not considered as a criterion to evaluate the most suitable process parameters. Although, this information shows again that the process is quite stable in most of the analyzed conditions. This result is also in good agreement with data available in literature [6, 33], in which low porosity values were achieved when using low powder feed rates (< 10 g/min).

Another important parameter to evaluate, when using a single scan approach, is the G-to-D ratio. Capello et al. [34] explained how this parameter is a good mean in order to discern the energy spent to melt the deposited material from the energy used to melt the base material. Moreover, G/D is a good indicator of the metallurgical bond between

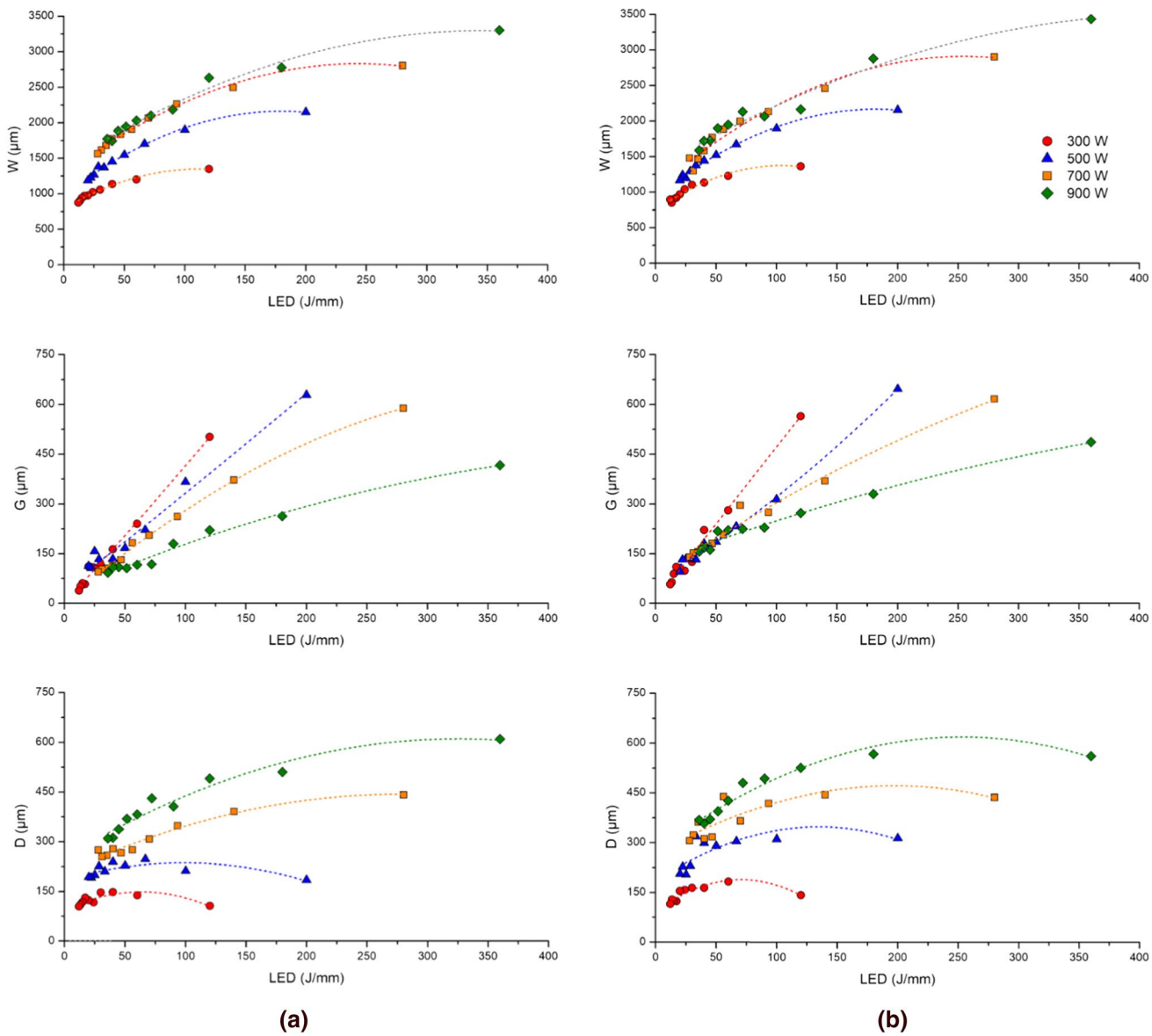

Fig. 4 Geometrical parameters (W, G, D) evaluations for the ArS0 **a** and ArS15 **b** specimens

the deposited material and the baseplate. They also provide a threshold value of 1, over which the bond created is not strong enough from a metallurgical point of view, hence must be avoided. Substantially, if G/D > 1, the growth of a layer exceeds the ability of the laser to completely remelt the previously deposited layer (or baseplate) during a DED process. This phenomenon might lead to undesired phenomena such as layer debonding and pores/cracks formation, as stated by Peng et al. [11]. G/D was evaluated for all the samples subject of this study, as illustrated in Fig. 5.

In both conditions, most of the samples showed a G/D ratio lower than 1, although some specimens exceeded this threshold value, more likely if built using a low laser power. Consequently, a higher power grants more freedom of changing scanning speed without compromising the possibility to build 3D objects. Furthermore, the ArS0 samples (Fig. 5a) showed higher maximum G/D value in correspondence of lower laser power values (300 W, 500 W), which was the consequence of the stronger effect of the shielding gas on D. In fact, as G was basically unaffected by argon flow at lower power, D instead decreased if the samples were not fully protected (Fig. 4).

In order to provide another parameter useful to determine the most proper process parameters window and to further optimize the process, the powder efficiency (P_e) of all the samples was investigated. This value can be used to estimate the amount of powder effectively delivered and melted on the substrate, as a function of the powder

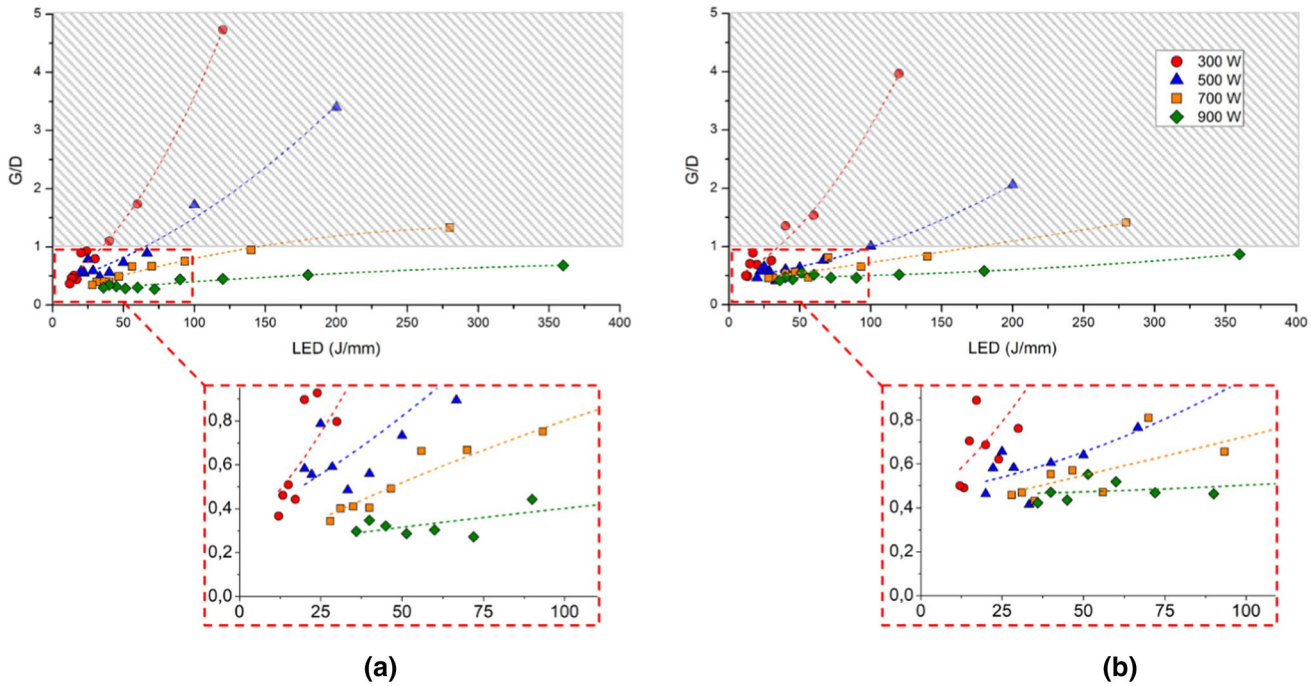

Fig. 5 G/D ratio evaluated on ArS0 **a** and ArS15 **b** samples. The dashed area represents the range in which G/D < 1

mass flow during the process. Of course, higher values are preferred, thus leading to low material waste during deposition. De Oliveira et al. [35] calculated P_e using the following equation:

$$P_e = 100 \cdot \frac{A_c \cdot v \cdot \rho_p}{F} [\%] \quad (3)$$

where A_c is the top part of the scan area from the cross-section (Fig. 3), ρ_p is the powder density (4.43 g/cm^3), and F is the powder feed rate.

The trends evaluated for both shielding conditions, available in Fig. 6, show a marked increase in powder efficiency as the laser power increased. An increase in LED had a more significant beneficial effect on P_e at lower laser power values.

The comparison of the P_e of the different building scenarios showed that in ArS0 samples the efficiency lies below 60% for most samples, unless the highest *P* value was used (900 W) (Fig. 6a). The maximum efficiency detected was 70.9% for the specimen built using a LED of 180 J/mm (900 W, 300 mm/min). In the additional shielding scenario (Fig. 6b), P_e was comparable with the former case, hence being mostly limited below the 60% value. However, in this case, the exceptions lay in the high-LED 700 W samples and the 900 W samples. The maximum efficiency detected

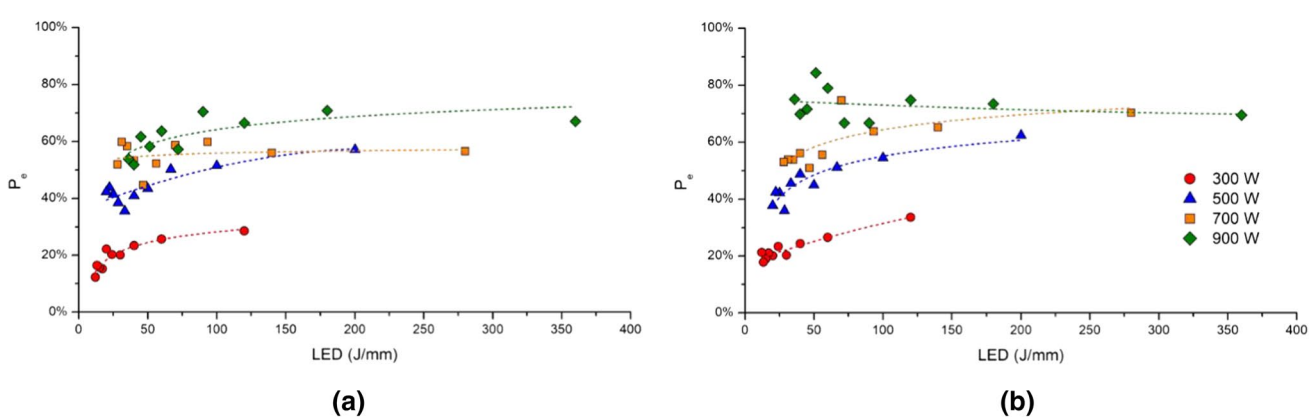

Fig. 6 Powder efficiency evaluated on ArS0 **a** and ArS15 **b** scans

was 84.3% for the specimen built using a LED of 51.4 J/mm (900 W, 1050 mm/min). Then, the additional shielding gas flow seem to have a beneficial effect of the samples built using higher *P* values.

In order to better analyze the differences between samples built in different shielding conditions, the ΔP_e parameter was investigated and plotted in Fig. 7. This index represents the difference in efficiency between the two shielding scenarios and is calculated as:

$$\Delta P_e = P_e^{shielding} - P_e^{notshielding} \tag{4}$$

Figure 7 shows that the beneficial effect of using the additional shielding gas system was marginal for low laser powers. In fact, the ΔP_e values associated with the 300 W and 500 W specimens ranged between 5% and 10%. A more significant rise in the powder efficiency of the Ars15 samples was detected for P = 700 W. In this case ΔP_e is shifted towards higher values, reaching an increase ≥ 10% for the higher-LED samples. Instead, for the highest laser power considered (900 W), the increase in efficiency appeared evident, especially for lower LED (< 75 J/mm). In correspondence of this values, multiple samples showed ΔP_e values ranging from a minimum of 10% to a maximum higher than 25%. Moreover, these samples corresponded to the overall highest P_e values (Fig. 6). Confirming that the additional shielding gas has a more beneficial effect on samples built using a higher laser power, especially if lower energy densities are used.

It must be taken into consideration that P_e depends on different parameters:

$$P_e = f(A_c, v, \rho_p, F) \tag{5}$$

Although, during the comparison between shielding scenarios in which ΔP_e was calculated, the specimens built using the same parameters were compared and since F and ρ_p were considered as constant, then ΔP_e is exclusively a function of the geometrical feature A_c in this analysis. Mazzucato et al. [25] encountered a similar P_e behavior when studying Ti-6Al-4V produced by means of DED. In their study, an increment in the deposition efficiency was encountered when deploying an additional shielding gas system, that allowed a more effective concentration of the powder flow, allowing to deliver a greater amount of powder in the melting area. A similar behavior was encountered in this analysis, as proved by the on-top view of the scans built using P = 100 W and v = 750 mm/min, illustrated in Fig. 8. These samples were already labelled as characterized by unacceptable process parameters, as in fact no powder melting occurred. Although, the lack of an actual scan granted the possibility to study more effectively how the powder behaved during the deposition, by considering the particles that partially melted and adhered to the substrate. A greater powder concentration in the central part of the scan, when the additional shielding was used, resulted quite clear. Instead, in the other case, the

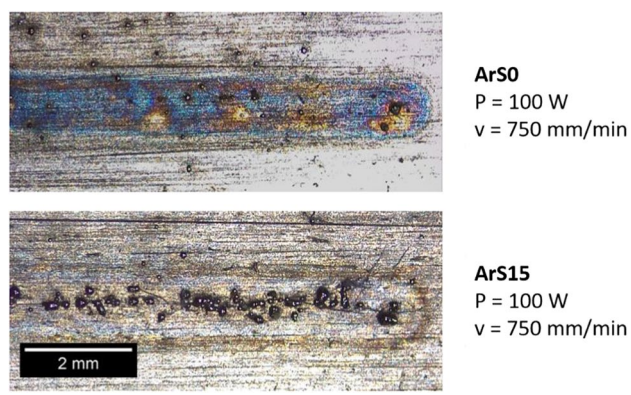

Fig. 8 On-top view of two scans built using the same process parameters, but with different shielding

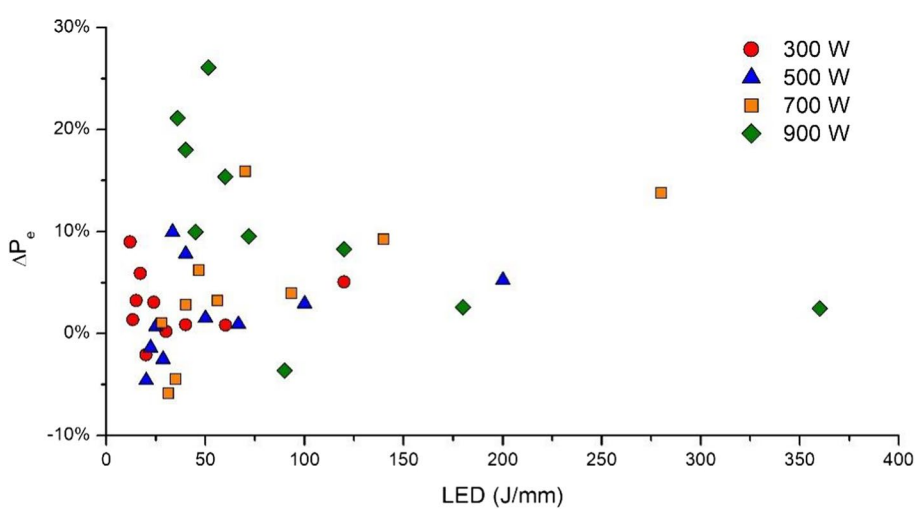

Fig. 7 Difference in powder efficiency between the two shielding scenarios

particles appeared quite sparse and definitely less concentrated. The beneficial effect of the additional shielding gas system was due to augmented overall gas flow of the overall apparatus (shielding gas system + carrier gas system), which reduced the possibility for the powder to flow outside of the melting area, accordingly to the results found in literature.

Furthermore, studying the microstructure of the single scans, useful information to determine the effect of the process parameters on the material microstructure were obtained.

From a microstructural point of view, all the samples showed a prior β-grain columnar morphology, a typical outcome for DED technology [36]. The related microstructures were mainly martensitic (α'), recognizable by the typical α' needles [17, 37]. Although, in order to elaborate data, a procedure to numerically quantify this type of microstructure was needed. The results of this evaluation (Fig. 9) showed a clear downward sloping trend for higher LED values both for representative samples built using low power (300 W in the graph) and high power (700 W in the graph), in both shielding scenarios. In titanium alloys, martensite formation is strictly dependent on the cooling rate that the sample undergoes, if the initial temperature is above T_β (β transition temperature), approximately 995 °C [17] for Ti-6Al-4V. During deposition, the cooling rate is high enough to allow martensite formation [38], although the dimension of the α' needles is again strictly dependent on several conditions, most importantly cooling rate [37, 39]. This value is directly correlated to the energy density used during the process. In particular, higher LED values deployed during the deposition lead to a lower cooling rate [40]. Therefore, evaluating martensitic size is very important, as it has a direct impact on several material properties, such as mechanical properties [41]. In fact, α' is an embrittling phase in titanium alloys, due to its efficiency at hindering dislocation motion [42]. Consequently, being able to control its size is a useful tool in order to tailor the mechanical properties of the final component [37].

An inverse correlation between α' size (width) and LED (cooling rate) was found in this work, hence samples characterized by a finer martensitic microstructure (lower α' spacing) were linked to a building process in which the cooling rate was lower. The results of the current investigation are in good agreement with a previous study from the authors [21]. In fact, higher LED samples, characterized by a lower α' spacing, hence a finer microstructure, are correlated to lower cooling rates, as proved by Yan et al. [40].

When comparing the data of ArS0 and ArS15 samples (Fig. 9a and b), even if the trends were similar, the former showed a finer microstructure. This phenomenon was possibly related to interstitial elements (mostly oxygen and nitrogen) pick-up, which can be reasonably assumed to be more relevant when the additional shielding is not used. These elements fit well in the hcp lattice of the α-phase in titanium alloys, causing embrittlement, a M_s (martensite start temperature) slight increase and a conspicuous rise of T_β [43]. This changes mutate the formation dynamics of α' and its size, by increasing the temperature range that lies between T_β and M_s during cooling, thus favoring the β → α + β transformation during cooling from the molten state. This set of data is also in good agreement with a previous work [21], in which the samples characterized by a higher interstitials concentration were found to have a finer martensitic microstructure, in which α + β was detected alongside α'. The microstructure appears therefore to be a good indicator of the interstitial content in the alloy.

To further investigate the previously mentioned β phase formation, which acts in contrast of the β → α' transformation, and to confirm the assumptions made above, an in-depth microstructural analysis was conducted. To do so, specimens built using the same process parameters (P, v) were compared in order to understand the impact of the additional shielding gas on the final microstructure of the

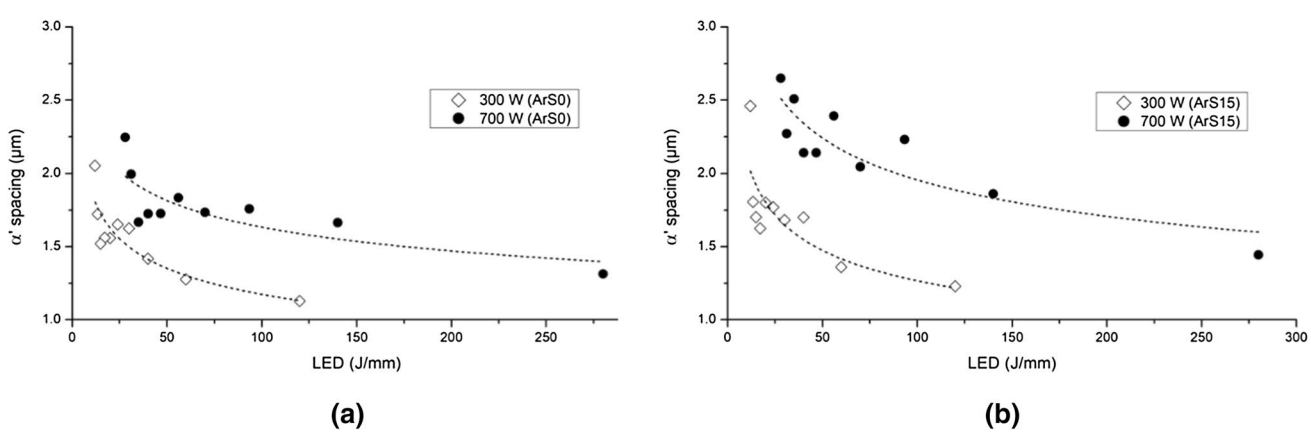

Fig. 9 Representative α' spacing trends evaluated on ArS0 **a** and ArS15 **b** single scans, built using a P of 300 W and 700 W

single track (Fig. 10). All the ArS15 (representative image in Fig. 10d) provided a mainly martensitic microstructure, in which only a very negligible amount of traces of $\alpha+\beta$ were found. However, most of the ArS0 samples (representative image in Fig. 10) were characterized by the mixed microstructure mentioned before, in which martensitic needles lay on a $\alpha+\beta$ fine lamellar matrix. This phenomenon was evident when comparing the microstructure of the single scan and its HAZ (heat affected zone). The ArS0 scan microstructure (Fig. 10b) greatly differed from the one of its HAZ (Fig. 10c), which appeared completely martensitic. Oppositely, the ArS15 samples showed a very similar microstructure in the bulk area (Fig. 10e) and the HAZ (Fig. 10f), which appeared martensitic as well. Both these areas recrystallized due to the high input energy of the laser that caused a rise in temperature above T_β. Although only the area created by the melting of the feedstock powder shows a mixed microstructure. In fact, the HAZ was heated at a peak temperature T_{HAZ} such that $T_\beta < T_{HAZ} < T_m$ (melting temperature). The single scan instead, reached a peak temperature T_{SS} such that $T_m < T_{SS}$ [44]. Oxygen pick-up and oxidation are phenomena consistently more rapid and effective in the molten state, as oxygen can effectively disperse throughout the whole molten region [45]. This behavior confirms that an insufficient shielding gas flow may cause relevant changes in the sample, in terms of microstructure.

Although, the resulting micrographs showed the microstructure after one single deposition, while in a 3D component, multiple layers are deposited. By doing so, the effect of the complex cycle of heating and cooling every layer undergoes was neglected [39, 46]. Notwithstanding these considerations, microstructural investigation allows to design the process in order to maximize certain properties, such as strength or ductility.

Moreover, a previous work from the authors [21] suggested that the Ti-6Al-4V specimens built using DED systems, in which interstitials pick-up is high enough to cause a change in microstructure, are also characterized by a very brittle behavior, that eventually causes critical issues when producing actual 3D components, such as cracks and layer debonding. Hence, the additional shielding gas system must be used at all times in order to avoid the formation of such defects. When considering the final process window to process Ti-6Al-4V then, only the samples built using complementary argon flow were considered.

To sum-up, the following criteria must be considered in order to choose the most suitable process parameters to process this material:

- The samples built without using the additional shielding gas flow cannot be chosen, as a result of the investigation of the microstructure, which suggests an excessive enrichment of interstitials elements;
- Tthe samples built using P = 100 W must be rejected, due to their poor adhesion with the baseplate and the lack of acceptable degree of metallurgical bonding;
- The samples characterized by G/D > 1 are unacceptable, because multilayer components would be characterized by cracks and de-bonding.

The remaining acceptable combinations were still numerous (Fig. 11), proving once again the stability of this process for this specific alloy. Hence, there is a certain freedom of choice, in terms of process parameters. For example, higher *P* values resulted more promising in terms of powder efficiency, although a lower laser power allowed to produce samples characterized by a rougher microstructure (α' spacing), which might be beneficial in terms of processability. In fact, a tight martensitic spacing might hinder dislocation movement, embrittling the material and then lead to undesired process phenomena, such as debonding and cracking due to excessive thermal stress accumulation [37].

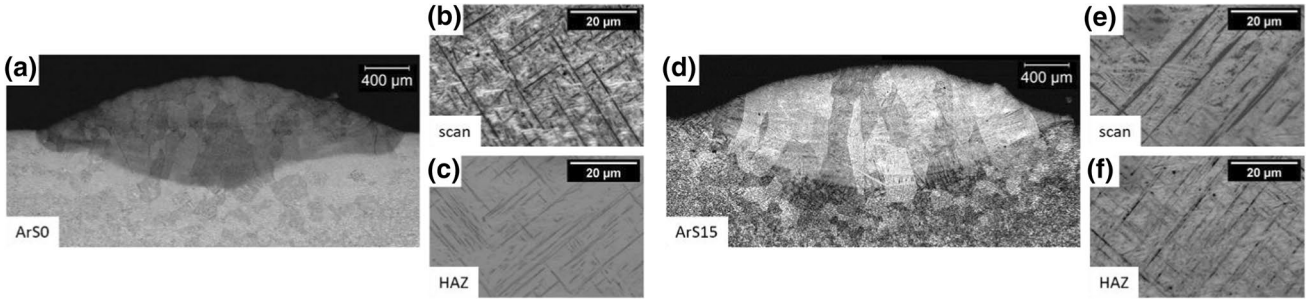

Fig. 10 Representative cross-section of an ArS0 sample **a** and relative micrographs of the scan **b** and the HAZ **c**; representative cross-section of an ArS15 sample **d** and relative micrographs of the scan **e** and the HAZ **f**. Both specimens share the same process parameters (P = 700 W, v = 300 mm/min)

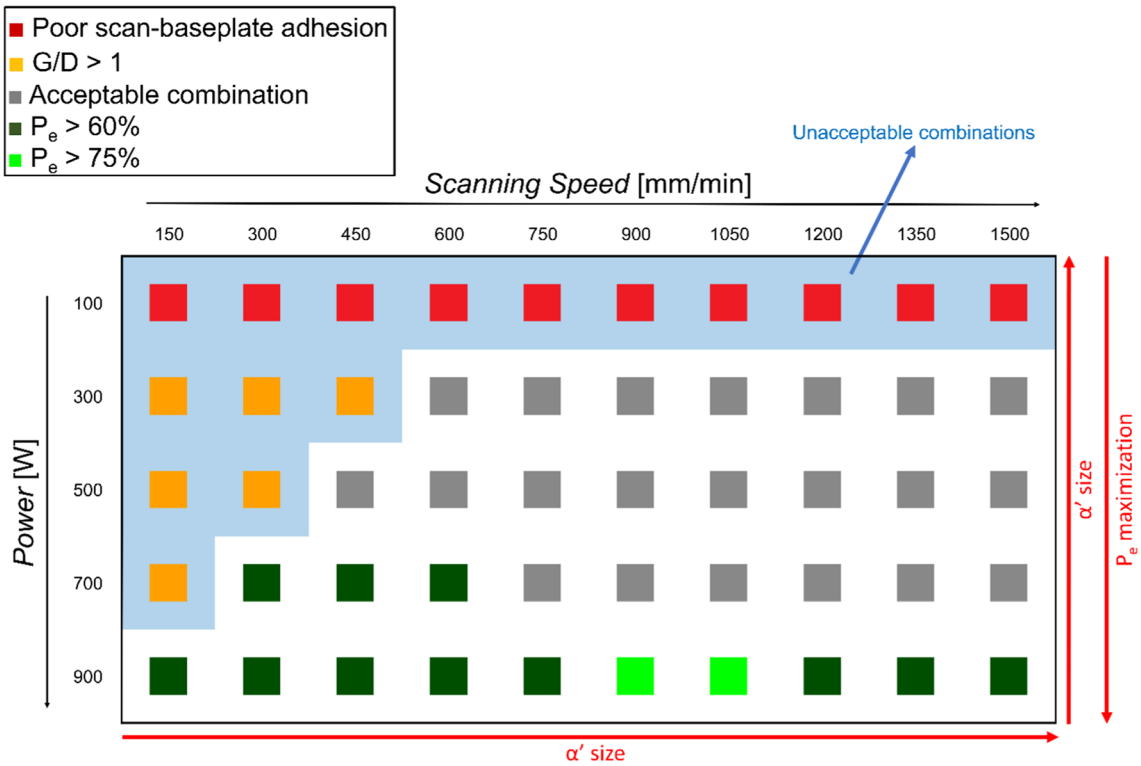

Fig. 11 Process parameters window for the samples built using additional argon flow in which every combination was color-coded according to the previous tests results

4 Conclusions

The aim of this work was to investigate how laser power, scanning speed and the use of an additional shielding affected the processability of Ti-6Al-4V produced by means of DED. Moreover, the most promising process window was evaluated and the effect of the process parameters on the microstructure was determined. The most significant results gathered can be summarized as follows:

- A laser power of 100 W was insufficient to fully melt the feedstock material and obtain a stable track, therefore a higher value was needed.
- The use of the additional shielding gas flow allowed to avoid undesired phenomena, such as oxygen pick-up and an extensive sample oxidation, which were unacceptable due to the excessive embrittlement of the material they induce.
- The G/D ratio proved to be a useful tool to determine some unacceptable process parameters combinations. In particular, it resulted more significant for excluding some combinations characterized by lower *P* and v values.
- The overall deposition process resulted more efficient for higher laser power values. The supplementary argon flow also lead to a higher powder efficiency, caused by a more effective concentration of the feedstock powder flow. The maximum powder efficiency was reached by the samples built using a P of 900 W and a v of 900–1050 mm/min.
- A correlation between the process parameters (LED) and microstructure was found. Even if martensite formation cannot be avoided, using the parameters subject of this study, α' spacing can be customized by conveniently choosing the process parameters. Finer microstructures resulted correlated with higher LED values.
- DED was demonstrated as a very stable technology to process Ti-6Al-4V, as an outcome of this investigation. In fact, it grants the user a lot of flexibility, in terms of acceptable process parameters choice. Moreover, an overall best combination was not found, as the process can be opportunely tailored, depending on the goal of the user (e.g. efficiency maximization or microstructural customization).

Acknowledgements The authors would like to acknowledge the European Horizon 2020 research and innovation program; grant agreement No. 723795 / 4D Hybrid–Novel ALL-IN-ONE machines, robots and systems for affordable, worldwide and lifetime distributed 3D hybrid manufacturing and repair operations. The authors would also like also

to express their appreciation for assistance provided by Dr. Fulvio Muscatello in data analyses.

Funding Open access funding provided by Politecnico di Torino within the CRUI-CARE Agreement. This work was funded by the European Horizon 2020 research and innovation program; grant agreement No. 723795 / 4D Hybrid–Novel ALL-IN-ONE machines, robots and systems for affordable, worldwide and lifetime distributed 3D hybrid manufacturing and repair operations.

Code availability Not applicable.

Compliance with Ethical Standards

Conflict of interest The authors declare no conflict of interest.

Open Access This article is licensed under a Creative Commons Attribution 4.0 International License, which permits use, sharing, adaptation, distribution and reproduction in any medium or format, as long as you give appropriate credit to the original author(s) and the source, provide a link to the Creative Commons licence, and indicate if changes were made. The images or other third party material in this article are included in the article's Creative Commons licence, unless indicated otherwise in a credit line to the material. If material is not included in the article's Creative Commons licence and your intended use is not permitted by statutory regulation or exceeds the permitted use, you will need to obtain permission directly from the copyright holder. To view a copy of this licence, visit http://creativecommons.org/licenses/by/4.0/.

References

1. W.E. Frazier, J. Mater. Eng. Perform. **23**, 1917–1928 (2014)
2. S.M. Thompson, L. Bian, N. Shamsaei, A. Yadollahi, Addit. Manuf. **8**, 36–62 (2015)
3. P.N. Sibisi, A.P.I. Popoola, N.K.K. Arthur, S.L. Pityana, Int. J. Adv. Manuf. Tech. **107**, 1163 (2020)
4. A. Gisario, M. Kazarian, F. Martina, M. Mehrpouya, J. Manuf. Syst. **53**, 124–149 (2019)
5. E. Brandl, D. Greitemeier, Mater. Lett. **81**, 84–87 (2012)
6. B.E. Carroll, T.A. Palmer, A.M. Beese, Acta Mater. **87**, 309–320 (2015)
7. Y. Huang, M.B. Khamesee, E. Toyserkani, Opt. Laser Technol. **109**, 584–599 (2019)
8. P.A. Kobryn, E.H. Moore, S.L. Semiatin, Scr. Mater. **43**, 299–305 (2000)
9. R. Cottam, M. Brandt, Physcs. Proc. **12**, 323–329 (2011)
10. R.M. Mahamood, E.T. Akinlabi, S. Akinlabi, Lasers Manuf. Mater. Process. **2**, 43–55 (2015)
11. L. Peng, Y. Taiping, L. Sheng, L. Dongsheng, H. Qianwu, X. Weihao, Z. Xiaoyan, Int. J. Mach. Tools Manuf. **45**, 1288–1294 (2005)
12. F. Mazzucato, A. Aversa, R. Doglione, S. Biamino, A. Valente, M. Lombardi, Metals **9**, 1160 (2019)
13. A. Aversa, M. Moshiri, F. Calignano, D. Manfredi, S. Tusacciu, M. Busatto, M. Lai, M. Lombardi, M. Pavese, S. Biamino, in *Proc. Euro PM 2017 Int. Powder Metall. Congr. Exhib.* (2017)
14. J. Gockel, J. Beuth, in *Solid Freeform Fabrication Proceedings*, 24th International Solid Freeform Fabrication Symposium - An Additive Manufacturing Conference, SFF 2013, Austin, August 12-14 2013 (The University of Texas, Austin, 2013), pp. 666–674
15. C. Katinas, S. Liu, Y.C. Shin, J. Manuf. Sci. E. T. ASME **141**, 1–10 (2019)
16. C. Cui, B.M. Hu, L. Zhao, S. Liu, Mater. Des. **32**, 1684–1691 (2011)
17. C. Leyens, M. Peters, *Titanium and Titanium Alloys: Fundamentals and Applications* (Wiley, New Jersey, 2003)
18. N.A. Kistler, D.J. Corbin, A.R. Nassar, E.W. Reutzel, A.M. Beese, J. Mater. Process. Tech. **264**, 172–181 (2019)
19. F. Trevisan, F. Calignano, A. Aversa, G. Marchese, M. Lombardi, S. Biamino, D. Ugues, D. Manfredi, J. Appl. Biomater. Funct. Mater. **16**, 57–67 (2018)
20. F.G. Arcella, F.H. Froes, JOM **52**, 28–30 (2000)
21. A. Carrozza, A. Aversa, F. Mazzucato, M. Lombardi, S. Biamino, A. Valente, P. Fino, Appl. Sci. **10**, 4212 (2020)
22. Y. Byun, S. Lee, S.-M. Seo, J. Yeom, S.E. Kim, N. Kang, J. Hong, Met. Mater. Int. **24**, 1213–1220 (2018)
23. O.G. Klimova-Korsmik, G.A. Turichin, S.A. Shalnova, M.O. Gushchina, V.V. Cheverikin, J. Phys. Conf. Ser. **1109**, 012061 (2018)
24. M. Gharbi, P. Peyre, C. Gorny, M. Carin, S. Morville, P. Le Masson, D. Carron, R. Fabbro, J. Mater. Process. Tech. **213**, 791–800 (2013)
25. F. Mazzucato, A. Marchetti, A. Valente, in *Industrializing Additive Manufacturing - Proceedings of Additive Manufacturing in Products and Applications - AMPA2017*, ed. by M. Meboldt, C. Klahn (Springer, Cham, 2018), pp. 59–69
26. M. Yan, W. Xu, M.S. Dargusch, H.P. Tang, M. Brandt, M. Qian, Powder Metall. **57**, 251–257 (2014)
27. G.F. Vander Voort, A. Roósz, Metallography **17**, 1–17 (1984)
28. H. Galarraga, R.J. Warren, D.A. Lados, R.R. Dehoff, M.M. Kirka, P. Nandwana, Mater. Sci. Eng. A **685**, 417–428 (2017)
29. Z. Jia, W. Zeng, Y. Zhang, C. Shi, B. Quan, J. Wu, J. Alloy. Compd. **640**, 488–496 (2015)
30. W. Peng, W. Zeng, Y. Zhang, C. Shi, B. Quan, J. Wu, J. Mater. Eng. Perform. **22**, 2588–2593 (2013)
31. J. Alcisto, A. Enriquez, H. Garcia, S. Hinkson, M. Hahn, J. Foyos, J. Ogren, E.W. Lee, O.S. Es-Said, Eng. Fail. Anal. **11**, 811–816 (2004)
32. AWS D17.1, Specification for Fusion Welding of Aerospace Applications (American Welding Society, Miami, 2001)
33. C. Qiu, G.A. Ravi, C. Dance, A. Ranson, S. Dilworth, M.M. Attallah, J. Alloy. Compd. **629**, 351–361 (2015)
34. E. Capello, B. Previtali, J. Mater. Process. Tech. **174**, 223–232 (2006)
35. U. de Oliveira, V. Ocelík, J.T.M. De Hosson, Surf. Coat. Tech. **197**, 127–136 (2005)
36. S. Gorsse, C. Hutchinson, M. Gouné, R. Banerjee, Sci. Technol. Adv. Mater. **18**, 584–610 (2017)
37. J. Yang, H. Yu, J. Yin, M. Gao, Z. Wang, X. Zeng, Mater. Des. **108**, 308–318 (2016)
38. G. Suprobo, A.A. Ammar, N. Park, E.R. Baek, S. Kim, Met. Mater. Int. **25**, 1428–1435 (2019)
39. E. Salsi, M. Chiumenti, M. Cervera, Metals **8**, 633 (2018)
40. L. Yan, L. Hill, J.W. Newkirk, F. Liou, in *Solid Freeform Fabrication 2017: Proceedings of the 28th Annual International Solid Freeform Fabrication Symposium – An Additive Manufacturing Conference*, Austin, August 7–9, 2017 (University of Texas, Austin, 2017), pp. 1846–1852
41. K. Wei, Z. Wang, F. Li, H. Zhang, X. Zeng, J. Alloy. Compd. **774**, 1024–1035 (2019)
42. M. Simonelli, Y.Y. Tse, C. Tuck, Mater. Sci. Eng. A **616**, 1–11 (2014)
43. S. Malinov, W. Sha, Z. Guo, Mater. Sci. Eng. A **283**, 1–10 (2000)
44. C.L. Erhard, V. Brandl, B. Michailov, Viehweger, Surf. Coat. Tech. **206**, 1–4 (2018)

45. X. Xu, J. Ding, S. Ganguly, C. Diao, S. Williams, J. Mater. Process. Tech. **252**, 739–750 (2018)
46. S.M. Kelly, S.L. Kampe, Metall. Mater. Trans. A **35**, 1869–1879 (2004)

Publisher's Note Springer Nature remains neutral with regard to jurisdictional claims in published maps and institutional affiliations.